

## Second-order nonlinear optical susceptibility of a quantum well with an applied electric field

Leung Tsang

*Department of Electrical Engineering (FT-10), University of Washington, Seattle, Washington 98195*

Shun-Lien Chuang and Shing M. Lee

*Department of Electrical and Computer Engineering, University of Illinois at Urbana-Champaign, 1406 West Green Street, Urbana, Illinois 61801-2991*

(Received 23 June 1989)

The second-order nonlinear optical susceptibility of a quantum well with an applied electric field is studied theoretically with use of both a parabolic-band model and a valence-band-mixing model. The electronic properties of the asymmetric quantum-well system due to an applied electric field and their effects on the second-order nonlinear susceptibility are illustrated. It is shown that the applied electric field may change the second-order susceptibility significantly. The dispersion of the nonlinear susceptibility using the valence-band-mixing model also shows more features than that using the simple parabolic-band model of previous studies of quantum-well systems.

### I. INTRODUCTION

Very interesting electronic and optical properties of the semiconductor quantum-well systems have been proposed<sup>1-3</sup> and investigated recently. For example, resonant-tunneling<sup>3-5</sup> and electroabsorption<sup>6,7</sup> effects in quantum-well structures have been demonstrated. Novel optoelectronic devices using quantum-well structures such as semiconductor lasers,<sup>8,9</sup> photodetectors,<sup>10-12</sup> and electro-optical modulators<sup>13</sup> have been studied. Many interesting quantum-mechanical phenomena using such structures have been predicted and confirmed experimentally.

Nonlinear optical properties of semiconductor quantum wells have also been investigated recently for both interband<sup>14-16</sup> and intersubband transitions.<sup>17-19</sup> For interband transitions, exciton absorption saturation has also been investigated.<sup>20,21</sup> Nonlinear optical processes associated with generations of virtual carriers in an electric-field-biased quantum well by optical radiation with energy below the band-gap absorption edge have also been proposed.<sup>22,23</sup> These processes can also be understood from the nonlinear-optics theory as optical rectification. Ultrahigh-speed resonance using such an effect is expected since no true carriers are generated; thus, the response is not limited by the carrier lifetimes. A general feature of these interband and intersubband nonlinear processes is that very large nonlinearity is possible. This leads to the designs of novel nonlinear optoelectronic devices such as the self-electro-optical effect devices.<sup>13,24,25</sup>

In a symmetric quantum-well structure, the second-order nonlinear susceptibility is usually very small except for the contribution of the bulk susceptibility. Using a built-in asymmetric quantum-well system, such as graded wells or two coupled asymmetric wells, or a symmetric quantum well with an external applied electric field, a large second-order susceptibility becomes possible.<sup>26-28</sup>

Previous work on the second-order susceptibility using the intraband and intersubband transitions has been done using a parabolic band-structure model.<sup>16,27</sup> Furthermore, for interband second-order nonlinear susceptibility, the electric field effect has not been evaluated. On the other hand, the nonlinear optical susceptibility for bulk semiconductors such as GaAs and InAs has been calculated<sup>29-32</sup> using different methods, such as the empirical pseudopotential method and the tight-binding band-structure technique.

In this paper, we investigate the second-order nonlinear optical susceptibility of a quantum well with an external bias voltage using both the parabolic-band model and the valence-band-mixing model. Since we are interested in the optical energy near the band gap, the electronic structures based on the multiband effective-mass theory using the  $\mathbf{k}\cdot\mathbf{p}$  method<sup>33,34</sup> are calculated. The exciton effects are not included.<sup>16</sup> However, the inclusion of the exciton effects, although it does not affect the major conclusion of this paper, will make our model more complete. A completeness relation for the envelope functions in both the parabolic-band and valence-band-mixing models is used in the evaluation of the second-order susceptibility to speed up the convergence of the numerical results. We found that more features in the dispersion of the nonlinear susceptibility are present when the valence-band mixing is taken into account compared with that of the parabolic-band model. The interband nonlinear susceptibility is also significantly enhanced when an electric field is applied. Thus, electric field control of the second-harmonic generation using quantum-well structures will be very important.

### II. SECOND-HARMONIC GENERATION BASED ON THE PARABOLIC-BAND MODEL

Consider a quantum well grown along the [001] direction with a well thickness  $L_w$  and a barrier thickness  $L_B$

in an electric field  $\mathbf{F}$  applied in the direction perpendicular to the quantum-well layers (Fig. 1). We choose the origin to be at the center of the well. The Bloch wave function of the  $n$ th subband state in the quantum well is

$$\psi_n^b(\mathbf{k}_\parallel, \mathbf{r}) = e^{i\mathbf{k}_\parallel \cdot \mathbf{r}} \phi_n^b(z) u^b(\mathbf{r}), \quad (1)$$

where the superscript  $b$  is the band index and is equal to  $c$  (conduction band) or  $hh$  (heavy-hole band). The function

$$\chi_{xzx}^{(2)}(2\omega) = -\frac{|e|^3}{\hbar^2 V} \sum_{\mathbf{k}_\parallel, n, l, m} \left[ \frac{\langle \psi_m^{hh} | x | \psi_n^c \rangle \langle \psi_n^c | z | \psi_l^c \rangle \langle \psi_l^c | x | \psi_m^{hh} \rangle}{[2\omega - \omega_{hhm}^{cn}(\mathbf{k}_\parallel) + i\gamma_{hhm}^{cn}][\omega - \omega_{hhm}^{cl}(\mathbf{k}_\parallel) + i\gamma_{hhm}^{cl}]} - \frac{\langle \psi_m^{hh} | x | \psi_n^c \rangle \langle \psi_l^{hh} | z | \psi_m^{hh} \rangle \langle \psi_n^c | x | \psi_l^{hh} \rangle}{[2\omega - \omega_{hhm}^{cn}(\mathbf{k}_\parallel) + i\gamma_{hhm}^{cn}][\omega - \omega_{hhm}^{cl}(\mathbf{k}_\parallel) + i\gamma_{hhm}^{cl}]} \right], \quad (2)$$

where  $V$  is the volume of the crystal, and  $\gamma_b^a = (1/\tau_a + 1/\tau_b)/2$  is the linewidth parameter in the density-matrix formalism with  $\tau_a$  as the relaxation time for state  $a$ . In (2),  $\omega_{hhm}^{cn}(\mathbf{k}_\parallel) = [\epsilon_n^c(\mathbf{k}_\parallel) - \epsilon_m^{hh}(\mathbf{k}_\parallel)]/\hbar$  with  $\epsilon_n^c(\mathbf{k}_\parallel)$  and  $\epsilon_m^{hh}(\mathbf{k}_\parallel)$  being the  $n$ th bound-state energy of the conduction band and the  $m$ th bound-state energy of the heavy-hole band at the  $\mathbf{k}_\parallel$ , respectively. We also have

$$\epsilon_n^c(\mathbf{k}_\parallel) = E_n^c + \frac{\hbar^2 k_\parallel^2}{2m_c}$$

and

$$\epsilon_m^{hh}(\mathbf{k}_\parallel) = -E_g - E_m^{hh} - \frac{\hbar^2 k_\parallel^2}{2m_{hh}},$$

where  $E_g$  is the band-gap energy, and  $m_c$  and  $m_{hh}$  are the conduction-band and heavy-hole-band effective masses, respectively. The quantized subband energies  $E_n^c$  and  $E_m^{hh}$  are the energy eigenvalues for the envelope functions  $\phi_n^c$  and  $\phi_m^{hh}$ , respectively. In Eq. (2) of the parabolic-band model, the light-hole bands are neglected because the light-hole effective mass is comparable to that of the conduction-band mass and will result in a cancellation<sup>16</sup> of the corresponding two terms in Eq. (2). However, in the valence-band-mixing model to be discussed in Sec. III, the heavy-hole and light-hole bands are coupled so that such cancellation does not occur.

Using Kane's model, we have<sup>37-39</sup>

$$\langle \psi_m^{hh}(\mathbf{k}_\parallel) | x | \psi_n^c(\mathbf{k}_\parallel) \rangle = \frac{i \langle \phi_m^{hh} | \phi_n^c \rangle}{[\epsilon_n^c(\mathbf{k}_\parallel) - \epsilon_m^{hh}(\mathbf{k}_\parallel)]} \times \left[ \frac{\cos\theta_{cn}^{hhm} \cos\phi + i \sin\phi}{\sqrt{2}} \right] P, \quad (3)$$

where

$$P = \frac{\hbar}{\sqrt{2}} \left[ \frac{E_g(E_g + \Delta)}{m_c(E_g + 2\Delta/3)} \right]^{1/2} \quad (4)$$

$u^b(\mathbf{r})$  is the periodic part of the Bloch function and the remainder on the right-hand side of (1) is the envelope function. To derive the second-order susceptibility, the standard perturbation theory can be applied to the density-matrix formalism.<sup>35,36</sup> Assuming that the valence band is populated and the conduction band is empty and retaining only the resonant contributions for  $2\hbar\omega$  close to the band-gap energy give the following expression for the second-order susceptibility.

$$\cos\theta_{cn}^{hhm} = \left[ \frac{|E_n^c| + |E_m^{hh}|}{|E_n^c| + |E_m^{hh}| + E} \right]^{1/2}, \quad (5)$$

and  $E = \hbar^2 k_\parallel^2 / (2m_r)$  with  $1/m_r = 1/m_c + 1/m_{hh}$ , and  $\phi$  is the azimuthal angle of the  $(k_x, k_y)$  plane. Substituting (3)–(5) into (2), taking into account spin degeneracy,

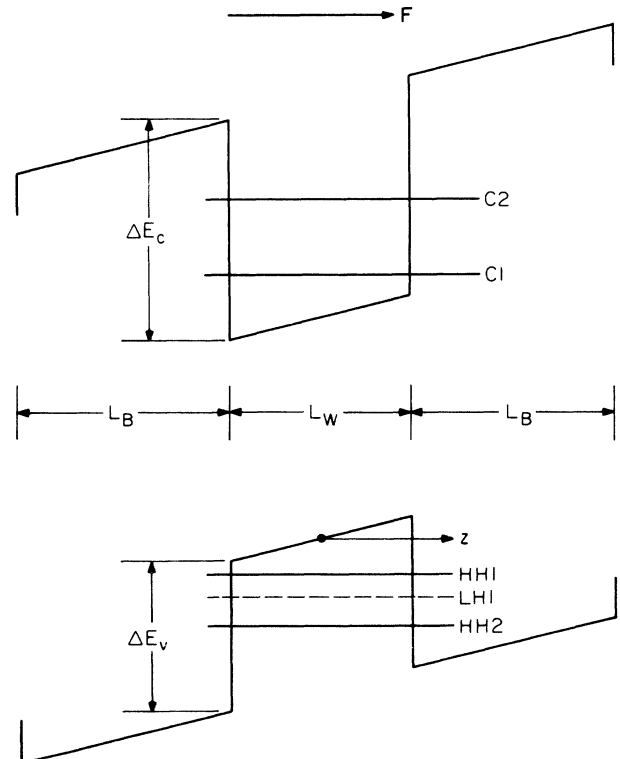


FIG. 1. A quantum well with an external applied electric field  $F$ .

changing summation over  $\mathbf{k}_\parallel$  into integration over  $d\mathbf{k}_\parallel = k_\parallel dk_\parallel d\phi$ , and performing the integration over  $d\phi$  give the result in terms of an integral over  $dk_\parallel$ . The in-

tegration variable  $k_\parallel$  can be further transformed to the integration variable  $E$ . We also note<sup>36</sup> that the second-harmonic coefficient  $d_{\text{zxx}}(2\omega) = \chi_{\text{zxx}}^{(2)}(2\omega)/2$ :

$$d_{\text{zxx}}(2\omega) = -\frac{|e|^3 P^2 m_r}{8\pi \hbar^2 L_s} \sum_{n,l,m} \int_0^{E_{\text{max}}} dE \left[ \frac{\langle \phi_m^{\text{hh}} | \phi_n^c \rangle \langle \phi_n^c | z | \phi_l^c \rangle \langle \phi_l^c | \phi_m^{\text{hh}} \rangle (1 + \cos\theta_{\text{cn}}^{\text{hhm}} \cos\theta_{\text{hhm}}^{\text{cl}})}{(E + E_{\text{hhm}}^{\text{cn}})(E + E_{\text{hhm}}^{\text{cl}})(2\hbar\omega - E_{\text{hhm}}^{\text{cn}} - E + i\hbar\gamma_{\text{hhm}}^{\text{cn}})} \right. \\ \times \frac{1}{(\hbar\omega - E_{\text{hhm}}^{\text{cl}} - E + i\hbar\gamma_{\text{hhm}}^{\text{cl}})} \\ \left. - \frac{\langle \phi_m^{\text{hh}} | \phi_n^c \rangle \langle \phi_l^{\text{hh}} | z | \phi_m^{\text{hh}} \rangle \langle \phi_n^c | \phi_l^{\text{hh}} \rangle (1 + \cos\theta_{\text{cn}}^{\text{hhm}} \cos\theta_{\text{hhm}}^{\text{cl}})}{(E + E_{\text{hhm}}^{\text{cn}})(E + E_{\text{hhm}}^{\text{cl}})(2\hbar\omega - E_{\text{hhm}}^{\text{cn}} - E + i\hbar\gamma_{\text{hhm}}^{\text{cn}})} \right. \\ \left. \times \frac{1}{\hbar\omega - E_{\text{hhm}}^{\text{cl}} - E + i\hbar\gamma_{\text{hhm}}^{\text{cl}}} \right], \quad (6)$$

where  $L_s = L_w + L_B$  and  $E_{\text{hhm}}^{\text{cn}} = E_g + E_n^c + E_m^{\text{hh}}$ . The result in (6) should be independent of the upper limit of integration  $E_{\text{max}}$  if the integral converges quickly. However, the integral in (6) is slowly convergent. The integrand has to decay faster than  $1/E$  for convergence to occur. For  $2\hbar\omega$  close to  $E_g$ , this means that the integral in (6) starts to converge for  $E > E_g$  which (i) makes numerical integration impractical and (ii) is beyond the regime of validity of the  $\mathbf{k} \cdot \mathbf{p}$  approximation. To speed up the convergence, we follow an approach similar to that used by Khurgin.<sup>16</sup> This is based on the assumption that both the conduction-band envelope functions  $\phi_l^c$  and the heavy-hole-band envelope functions  $\phi_l^{\text{hh}}$  form complete sets so that  $\sum_l |\phi_l^c\rangle \langle \phi_l^c| = \sum_l |\phi_l^{\text{hh}}\rangle \langle \phi_l^{\text{hh}}| = 1$ . Then in Eq. (6) we can subtract terms that add up to zero as follows:

$$d_{\text{zxx}}(2\omega) = -\frac{|e|^3 P^2 m_r}{8\pi \hbar^2 L_s} \sum_{n,l,m} \int_0^{E_{\text{max}}} dE \left[ \frac{\langle \phi_m^{\text{hh}} | \phi_n^c \rangle \langle \phi_n^c | z | \phi_l^c \rangle \langle \phi_l^c | \phi_m^{\text{hh}} \rangle}{(E + E_{\text{hhm}}^{\text{cn}})(2\hbar\omega - E_{\text{hhm}}^{\text{cn}} - E + i\hbar\gamma_{\text{hhm}}^{\text{cn}})} \right. \\ \times \left[ \frac{1 + \cos\theta_{\text{cn}}^{\text{hhm}} \cos\theta_{\text{hhm}}^{\text{cl}}}{(E + E_{\text{hhm}}^{\text{cl}})(\hbar\omega - E_{\text{hhm}}^{\text{cl}} - E + i\hbar\gamma_{\text{hhm}}^{\text{cl}})} \right. \\ \left. - \frac{1 + \cos\theta_{\text{cn}}^{\text{hhm}} \cos\theta_{\text{hhm}}^{\text{cn}}}{(E + E_{\text{hhm}}^{\text{cn}})(\hbar\omega - E_{\text{hhm}}^{\text{cn}} - E + i\hbar\gamma_{\text{hhm}}^{\text{cn}})} \right] \\ \left. - \frac{\langle \phi_m^{\text{hh}} | \phi_n^c \rangle \langle \phi_l^{\text{hh}} | z | \phi_m^{\text{hh}} \rangle \langle \phi_n^c | \phi_l^{\text{hh}} \rangle}{(E + E_{\text{hhm}}^{\text{cn}})(2\hbar\omega - E_{\text{hhm}}^{\text{cn}} - E + i\hbar\gamma_{\text{hhm}}^{\text{cn}})} \right. \\ \times \left[ \frac{1 + \cos\theta_{\text{cn}}^{\text{hhm}} \cos\theta_{\text{hhm}}^{\text{cl}}}{(E + E_{\text{hhm}}^{\text{cl}})(\hbar\omega - E_{\text{hhm}}^{\text{cl}} - E + i\hbar\gamma_{\text{hhm}}^{\text{cl}})} \right. \\ \left. - \frac{1 + \cos\theta_{\text{cn}}^{\text{hhm}} \cos\theta_{\text{hhm}}^{\text{cn}}}{(E + E_{\text{hhm}}^{\text{cn}})(\hbar\omega - E_{\text{hhm}}^{\text{cn}} - E + i\hbar\gamma_{\text{hhm}}^{\text{cn}})} \right] \Big]. \quad (7)$$

The second and fourth terms in (7) are the newly added terms. They are both independent of  $l$  aside from the factors  $\sum_l |\phi_l^c\rangle \langle \phi_l^c|$  and  $\sum_l |\phi_l^{\text{hh}}\rangle \langle \phi_l^{\text{hh}}|$ . Thus the two terms cancel each other using the completeness relations. The integrand in (7) starts to decay faster than  $1/E$  for  $E$  larger than the maximum of  $2\hbar\omega - E_g - E_n^c - E_m^{\text{hh}}$ ,  $|E_l^c - E_n^c|$ , and  $|E_l^{\text{hh}} - E_m^{\text{hh}}|$ . Thus, it starts to converge for  $E$  greater than the detuning energy and the intersubband energy separation, both of which are much smaller than the band-gap energy. We calculate  $d_{\text{zxx}}(2\omega)$  by direction integration of (7) until it converges. Unlike Khurgin,<sup>16</sup> who included only two subband states for the conduction band and the heavy-hole band, we have included all the tightly bound states for each band. The envelope functions are calculated by solving the one-dimensional Schrödinger equation in an external applied field using the finite-difference method.

A simple analytical expression can also be derived for an approximate solution of  $d_{\text{zxx}}(2\omega)$  using a method similar to that in Khurgin (Appendix A), where the product of two cosines has been replaced by its average value  $\frac{1}{3}$ . The result is

$$d_{\text{zxx}}(2\omega) = -\frac{|e|^3 P^2 m_r}{6\pi \hbar^2 L_s} \left[ \sum_{n,m} \sum_{l>n} \langle \phi_m^{\text{hh}} | \phi_n^c \rangle \langle \phi_n^c | z | \phi_l^c \rangle \langle \phi_l^c | \phi_m^{\text{hh}} \rangle (E_l^c - E_n^c) [I(E_{\text{hhm}}^{\text{cl}}) - I(E_{\text{hhm}}^{\text{cn}})] \right. \\ \left. - \sum_{n,m} \sum_{l>m} \langle \phi_m^{\text{hh}} | \phi_n^c \rangle \langle \phi_l^{\text{hh}} | z | \phi_m^{\text{hh}} \rangle \langle \phi_n^c | \phi_l^{\text{hh}} \rangle (E_l^{\text{hh}} - E_m^{\text{hh}}) [I(E_{\text{hhm}}^{\text{cl}}) - I(E_{\text{hhm}}^{\text{cn}})] \right], \quad (8)$$

where the function  $I(x)$  is listed in Eq. (A3) of Appendix A.

### III. SECOND-HARMONIC GENERATION BASED ON THE VALENCE-BAND-MIXING MODEL

In this model, we retain the simple isotropic parabolic band for the conduction band. For the valence band, we use the  $4 \times 4$  Luttinger-Kohn Hamiltonian, the elements of which are derived based on the  $\mathbf{k} \cdot \mathbf{p}$  method.<sup>40</sup> We also make a unitary transformation<sup>33,34,41</sup> of a  $4 \times 4$  Luttinger-Kohn Hamiltonian into a block-diagonal form with each block of dimension  $2 \times 2$ :

$$\underline{H} = \begin{pmatrix} \underline{H}^U & \underline{Q}_{2 \times 2} \\ \underline{Q}_{2 \times 2} & \underline{H}^L \end{pmatrix}, \quad (9)$$

where the upper and lower blocks,  $\underline{H}^U$  and  $\underline{H}^L$  are given by

$$\underline{H}^\sigma = - \begin{pmatrix} P \pm Q & \bar{R} \\ \bar{R}^\dagger & P \mp Q \end{pmatrix}, \quad (10)$$

where  $\sigma = U$  (or  $L$ ) refers to the upper (or lower)  $\pm$  signs

$$P = \frac{\hbar^2}{2m} \gamma_1 (k_\parallel^2 + k_z^2), \quad (11)$$

$$Q = \frac{\hbar^2}{2m} \gamma_2 (k_\parallel^2 - 2k_z^2), \quad (12)$$

$$\bar{R} = \frac{\sqrt{3}\hbar^2}{2m} \bar{\gamma} k_\parallel^2 - i \frac{\sqrt{3}\gamma_3 \hbar^2}{m} k_\parallel k_z, \quad (13)$$

where  $\bar{\gamma} = (\gamma_3 + \gamma_2)/2$ ,  $m$  is the free-electron mass, and  $\gamma_1, \gamma_2, \gamma_3$  are the Luttinger parameters. In the above equations, we have made use of the axial approximation<sup>33,34</sup> neglecting the warping of the bulk valence band in the  $(k_x, k_y)$  plane.

The wave functions for the upper and lower blocks are as follows:

$$\psi_{m\mathbf{k}_\parallel}^U(\mathbf{r}) = \sum_{\nu=1,2} g_m^{(\nu)}(\mathbf{k}_\parallel, z) e^{i\mathbf{k}_\parallel \cdot \rho} |\nu\rangle, \quad (14)$$

$$\psi_{m\mathbf{k}_\parallel}^L(\mathbf{r}) = \sum_{\nu=3,4} g_m^{(\nu)}(\mathbf{k}_\parallel, z) e^{i\mathbf{k}_\parallel \cdot \rho} |\nu\rangle, \quad (15)$$

where  $m$  denotes the  $m$ th quantized state. In (14) and (15),  $|\nu\rangle$  denotes the transformed basis set (Appendix B). The block envelope functions satisfy

$$\sum_{\nu=1,2} \left[ H_{\nu\nu'}^U \left[ \mathbf{k}_\parallel, -i \frac{\partial}{\partial z} \right] + V(z) \delta_{\nu\nu'} \right] g_m^{(\nu')}(\mathbf{k}_\parallel, z) = E_m^U(\mathbf{k}_\parallel) g_m^{(\nu)}(\mathbf{k}_\parallel, z), \quad (16)$$

$$\sum_{\nu=3,4} \left[ H_{\nu\nu'}^L \left[ \mathbf{k}_\parallel, -i \frac{\partial}{\partial z} \right] + V(z) \delta_{\nu\nu'} \right] g_m^{(\nu')}(\mathbf{k}_\parallel, z) = E_m^L(\mathbf{k}_\parallel) g_m^{(\nu)}(\mathbf{k}_\parallel, z), \quad (17)$$

where

$$V(z) = \begin{cases} |e|Fz, & |z| < L_w/2 \\ -\Delta E_v + |e|Fz, & |z| > L_w/2 \end{cases} \quad (18)$$

is the confining square-well potential in the bias field.

The second-order susceptibility is

$$\chi_{xzx}^{(2)}(2\omega) = - \frac{|e|^3}{4\pi^2 L_s \hbar^2} \int d\mathbf{k}_\parallel \left[ \sum_{\sigma_m, m} \sum_{\eta_l, l} \sum_{\eta_n, n} \frac{\langle \psi_m^{\sigma_m} | x | \psi_n^{c\eta_n} \rangle \langle \psi_n^{c\eta_n} | z | \psi_l^{c\eta_l} \rangle \langle \psi_l^{c\eta_l} | x | \psi_m^{\sigma_m} \rangle}{[2\omega - \omega_{\sigma_m m}^{c\eta_n n}(\mathbf{k}_\parallel) + i\gamma_{\sigma_m m}^{c\eta_n n}][\omega - \omega_{\sigma_m m}^{c\eta_l l}(\mathbf{k}_\parallel) + i\gamma_{\sigma_m m}^{c\eta_l l}]} \right. \\ \left. - \sum_{\sigma_m, m} \sum_{\sigma_l, l} \sum_{\eta_n, n} \frac{\langle \psi_m^{\sigma_m} | x | \psi_n^{c\eta_n} \rangle \langle \psi_l^{\sigma_l} | z | \psi_m^{\sigma_m} \rangle \langle \psi_n^{c\eta_n} | x | \psi_l^{\sigma_l} \rangle}{[2\omega - \omega_{\sigma_m m}^{c\eta_n n}(\mathbf{k}_\parallel) + i\gamma_{\sigma_m m}^{c\eta_n n}][\omega - \omega_{\sigma_l l}^{c\eta_n n}(\mathbf{k}_\parallel) + i\gamma_{\sigma_l l}^{c\eta_n n}]} \right], \quad (19)$$

where  $\eta_l = \uparrow$  or  $\downarrow$  for the spin of the bound state  $l$  in the conduction band and  $\sigma_m = U$  or  $L$  for the  $m$ th bound state of the valence band,  $\omega_{\sigma_m m}^{c\eta_n n}(\mathbf{k}_\parallel) = [\varepsilon_n^c(\mathbf{k}_\parallel) - \varepsilon_m^{\sigma_m}(\mathbf{k}_\parallel)]/\hbar$ ,  $\varepsilon_n^c(\mathbf{k}_\parallel)$  is the same as that for the parabolic-conduction band model, and  $\varepsilon_m^{\sigma_m}(\mathbf{k}_\parallel) = -E_g + E_m^{\sigma_m}(\mathbf{k}_\parallel)$ . The matrix elements in (19) are derived in Appendix C.

We next substitute the matrix elements of Appendix C in (19). The integration  $\int d\mathbf{k}_\parallel = \int k_\parallel dk_\parallel \int_0^{2\pi} d\phi$ , in which the  $d\phi$  integration can be carried out. The result is

$$\begin{aligned}
d_{\text{zxx}}(2\omega) = & -\frac{|e|^3 P^2}{8\pi L_s} \int_0^{k_{\parallel\text{max}}} dk_{\parallel} k_{\parallel} \left[ \sum_{n,l,m,\sigma_m} \frac{\langle \phi_n^c | z | \phi_l^c \rangle f(n,l,m,\sigma_m, k_{\parallel})}{\epsilon_{\sigma_m m}^{cn}(\mathbf{k}_{\parallel}) \epsilon_{\sigma_m m}^{cl}(\mathbf{k}_{\parallel})} \right. \\
& \times \frac{1}{[2\hbar\omega - \epsilon_{\sigma_m m}^{cn}(\mathbf{k}_{\parallel}) + i\hbar\gamma_{\sigma_m m}^{cn}][\hbar\omega - \epsilon_{\sigma_m m}^{cl}(\mathbf{k}_{\parallel}) + i\hbar\gamma_{\sigma_m m}^{cl}]} \\
& - \sum_{n,l,m,\sigma_m} \frac{w(n,l,m,\sigma_m, k_{\parallel})}{\epsilon_{\sigma_m m}^{cn}(\mathbf{k}_{\parallel}) \epsilon_{\sigma_m l}^{cn}(\mathbf{k}_{\parallel})} \\
& \left. \times \frac{1}{[2\hbar\omega - \epsilon_{\sigma_m m}^{cn}(\mathbf{k}_{\parallel}) + i\hbar\gamma_{\sigma_m m}^{cn}][\hbar\omega - \epsilon_{\sigma_m l}^{cn}(\mathbf{k}_{\parallel}) + i\hbar\gamma_{\sigma_m l}^{cn}]} \right], \tag{20}
\end{aligned}$$

where

$$\epsilon_{\sigma_m m}^{cn}(\mathbf{k}_{\parallel}) = \epsilon_n^c(\mathbf{k}_{\parallel}) - \epsilon_m^{\sigma}(\mathbf{k}_{\parallel}), \tag{21}$$

$$f(n,l,m,\sigma_m, k_{\parallel}) = \begin{cases} \langle g_m^{(1)}(\mathbf{k}_{\parallel}) | \phi_n^c \rangle \langle \phi_l^c | g_m^{(1)}(\mathbf{k}_{\parallel}) \rangle + \frac{1}{3} \langle g_m^{(2)}(\mathbf{k}_{\parallel}) | \phi_n^c \rangle \langle \phi_l^c | g_m^{(2)}(\mathbf{k}_{\parallel}) \rangle & \text{for } \sigma_m = U \\ \langle g_m^{(4)}(\mathbf{k}_{\parallel}) | \phi_n^c \rangle \langle \phi_l^c | g_m^{(4)}(\mathbf{k}_{\parallel}) \rangle + \frac{1}{3} \langle g_m^{(3)}(\mathbf{k}_{\parallel}) | \phi_n^c \rangle \langle \phi_l^c | g_m^{(3)}(\mathbf{k}_{\parallel}) \rangle & \text{for } \sigma_m = L, \end{cases} \tag{22}$$

$$w(n,l,m,\sigma_m, k_{\parallel}) = \begin{cases} \sum_{\nu=1,2} \langle g_l^{(\nu)}(\mathbf{k}_{\parallel}) | z | g_m^{(\nu)}(\mathbf{k}_{\parallel}) \rangle [\langle g_m^{(1)}(\mathbf{k}_{\parallel}) | \phi_n^c \rangle \langle \phi_n^c | g_l^{(1)}(\mathbf{k}_{\parallel}) \rangle \\ \quad + \frac{1}{3} \langle g_m^{(2)}(\mathbf{k}_{\parallel}) | \phi_n^c \rangle \langle \phi_n^c | g_l^{(2)}(\mathbf{k}_{\parallel}) \rangle] & \text{for } \sigma_m = U \\ \sum_{\nu=3,4} \langle g_l^{(\nu)}(\mathbf{k}_{\parallel}) | z | g_m^{(\nu)}(\mathbf{k}_{\parallel}) \rangle [\langle g_m^{(4)}(\mathbf{k}_{\parallel}) | \phi_n^c \rangle \langle \phi_n^c | g_l^{(4)}(\mathbf{k}_{\parallel}) \rangle \\ \quad + \frac{1}{3} \langle g_m^{(3)}(\mathbf{k}_{\parallel}) | \phi_n^c \rangle \langle \phi_n^c | g_l^{(3)}(\mathbf{k}_{\parallel}) \rangle] & \text{for } \sigma_m = L. \end{cases} \tag{23}$$

In (20), the integral will be independent of the upper limit  $k_{\parallel\text{max}}$  if the integral converges quickly. However, as in the parabolic-band model case of (6), the integral in (20) converges slowly. To speed up the convergence, we follow the same idea as in the parabolic-band model case and assume the following completeness relations. For the conduction band,  $\sum_l |\phi_l^c\rangle \langle \phi_l^c| = 1$ . For the upper Hamiltonian of the valence band,  $\sum_l |g_l^{(\nu_1)}(\mathbf{k}_{\parallel})\rangle \langle g_l^{(\nu_2)}(\mathbf{k}_{\parallel})| = \delta_{\nu_1\nu_2}$  with  $\nu_1, \nu_2 = 1, 2$ . For the lower Hamiltonian of the valence band,  $\sum_l |g_l^{(\nu_3)}(\mathbf{k}_{\parallel})\rangle \langle g_l^{(\nu_4)}(\mathbf{k}_{\parallel})| = \delta_{\nu_3\nu_4}$ , with  $\nu_3, \nu_4 = 3, 4$ . Then we can subtract terms that add up to zero from (20), which results in

$$\begin{aligned}
d_{\text{zxx}}(2\omega) = & -\frac{|e|^3 P^2}{8\pi L_s} \int_0^{k_{\parallel\text{max}}} dk_{\parallel} k_{\parallel} \left[ \sum_{n,l,m,\sigma_m} \frac{\langle \phi_n^c | z | \phi_l^c \rangle f(n,l,m,\sigma_m, k_{\parallel})}{\epsilon_{\sigma_m m}^{cn}(\mathbf{k}_{\parallel}) [2\hbar\omega - \epsilon_{\sigma_m m}^{cn}(\mathbf{k}_{\parallel}) + i\hbar\gamma_{\sigma_m m}^{cn}]} \right. \\
& \times \left( \frac{1}{\epsilon_{\sigma_m m}^{cl}(\mathbf{k}_{\parallel}) [\hbar\omega - \epsilon_{\sigma_m m}^{cl}(\mathbf{k}_{\parallel}) + i\hbar\gamma_{\sigma_m m}^{cl}]} \right. \\
& \quad \left. - \frac{1}{\epsilon_{\sigma_m m}^{cn}(\mathbf{k}_{\parallel}) [\hbar\omega - \epsilon_{\sigma_m m}^{cn}(\mathbf{k}_{\parallel}) + i\hbar\gamma_{\sigma_m m}^{cn}]} \right) \\
& - \sum_{n,l,m,\sigma_m} \frac{w(n,l,m,\sigma_m, k_{\parallel})}{\epsilon_{\sigma_m m}^{cn}(\mathbf{k}_{\parallel}) [2\hbar\omega - \epsilon_{\sigma_m m}^{cn}(\mathbf{k}_{\parallel}) + i\hbar\gamma_{\sigma_m m}^{cn}]} \\
& \times \left( \frac{1}{\epsilon_{\sigma_m l}^{cn}(\mathbf{k}_{\parallel}) [\hbar\omega - \epsilon_{\sigma_m l}^{cn}(\mathbf{k}_{\parallel}) + i\hbar\gamma_{\sigma_m l}^{cn}]} \right. \\
& \quad \left. - \frac{1}{\epsilon_{\sigma_m m}^{cn}(\mathbf{k}_{\parallel}) [\hbar\omega - \epsilon_{\sigma_m m}^{cn}(\mathbf{k}_{\parallel}) + i\hbar\gamma_{\sigma_m m}^{cn}]} \right) \left. \right]. \tag{24}
\end{aligned}$$

The two new terms in (24) compared with (20) can be shown to cancel each other by using the completeness relations of the envelope functions. The integral in (24) converges much faster than that of (20) for reasons similar to that of the parabolic-band model.

#### IV. NUMERICAL RESULTS AND DISCUSSION

In this section we illustrate the numerical results of a  $\text{Ga}_{0.6}\text{Al}_{0.4}\text{As-GaAs}$  quantum well for  $2\hbar\omega$  between 1.28 and 1.68 eV. We have assumed the following set of parameters:  $E_g = 1.42$  eV,  $\Delta E_c = 0.2843$  eV, and  $\Delta E_v = 0.2144$  eV and the spin-split-off parameter  $\Delta = 0.343$  eV. This corresponds to a 57% band-gap-offset parameter. We have used a relaxation time of  $1.4 \times 10^{-13}$  sec so that  $\Gamma = \hbar\gamma = 4.7$  meV. The effective mass for the conduction band is  $m_c = 0.067m_0$ , where  $m_0$  is the electronic mass. In the parabolic-band model, we have used  $m_{hh} = 0.4537m_0$  for the effective mass of the heavy-hole band. In the valence-band-mixing model, we used the values  $\gamma_1 = 6.85$ ,  $\gamma_2 = 2.1$ , and  $\gamma_3 = 2.9$  for the Luttinger parameters.<sup>34</sup> The differences between these parameters in the GaAs and  $\text{Al}_x\text{Ga}_{1-x}\text{As}$  regions are ignored for simplicity since their effects on the lowest bound states are negligible.

In the parabolic-band model, we use the finite-difference method to solve the one-dimensional Schrödinger equation for the subband energies and the envelope function  $\phi_n^c$  of the conduction band and  $\phi_m^{hh}$  of the valence band. In the finite-difference method, we have placed reflecting walls at  $z = \pm(L_w/2 + L_B)$ . All the bound states of the conduction band and the heavy-hole band are included in (7) and (8). In Eq. (7), we performed the integration over  $dE$  numerically. The upper limit of integration,  $E_{\max}$ , is chosen such that the integral converges. The integral converges faster if  $2\hbar\omega$  is close to the band-gap energy  $E_g$  and slower as  $2\hbar\omega$  deviates farther from the band-gap energy. For the parameters that we have used, we found that the integration is sufficiently accurate for  $k_{\parallel\max} \approx 0.1 \text{ \AA}^{-1}$  and  $E_{\max} = \hbar^2 k_{\parallel\max}^2 / (2m_c) = 0.64$  eV.

In the valence-band-mixing model, we solved Eqs. (16) of the upper Hamiltonian and (17) of the lower Hamiltonian by using the finite-difference method. Equations (16) and (17) are solved for each  $k_{\parallel}$  and the subband energies  $\epsilon_m^{\sigma m}(\mathbf{k}_{\parallel})$  and envelope functions  $g_m^{(\nu)}(\mathbf{k}_{\parallel}, z)$  are calculated. All the bound states are included in the calculation. In calculating  $d_{xxx}(2\omega)$  by using Eq. (24), we performed the integration over  $dk_{\parallel}$  numerically until the integral converges. For the parameters of this paper, a choice of  $k_{\parallel\max} = 0.1 \text{ \AA}^{-1}$  gives sufficient accuracy. In performing the numerical integration of (24), the sharply peaked factor in the integrand is the resonant term of  $[2\hbar\omega - \epsilon_{\sigma m}^{cn}(\mathbf{k}_{\parallel}) + i\hbar\gamma]^{-1}$ . The other factors such as  $\epsilon_{\sigma m}^{cn}(\mathbf{k}_{\parallel})$ ,  $f(n, l, m, \sigma_m, k_{\parallel})$ , and  $w(n, l, m, \sigma_m, k_{\parallel})$  are smoothly varying over the domain  $0 < k_{\parallel} < k_{\parallel\max}$ . To speed up computation, these factors, which are computationally intensive, are only calculated at a selected num-

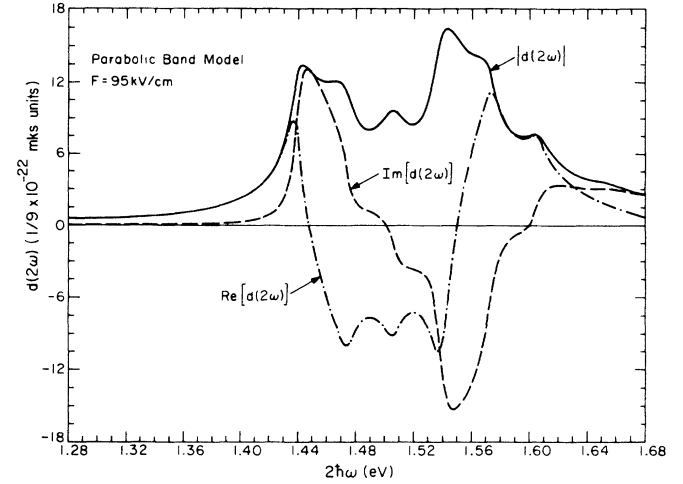


FIG. 2. The second-harmonic coefficient  $d(2\omega)$  ( $\frac{1}{9} \times 10^{-22}$  mks units) as a function of  $2\hbar\omega$  (eV) for a quantum well with a width  $L_w = 100 \text{ \AA}$ , and  $L_w + L_B = 152 \text{ \AA}$ .  $F = 95$  kV/cm. The parabolic-band model of Eq. (7) is used. The real part, imaginary part, and absolute values of  $d(2\omega)$  are illustrated.

ber of  $k_{\parallel}$ 's with the value at the rest of the  $k_{\parallel}$ 's calculated by a cubic spline interpolation.

In Fig. 2, the second-harmonic coefficient  $d(2\omega)$ , as computed by Eq. (7) of the parabolic-band model is plotted against  $2\hbar\omega$  for a QW of  $L_w = 100 \text{ \AA}$  in an external field of 95 kV/cm. The barrier width  $L_B$  is chosen as 52  $\text{\AA}$  so that there is negligible tunneling between wells. Outside the resonance region,  $|d(2\omega)|$  and  $\text{Re}[d(2\omega)]$  are practically indistinguishable. The first resonance occurs at the C1-HH1 transition (see Fig. 1), while the resonances at larger  $2\hbar\omega$  correspond to resonances at higher-order subband transitions. In Fig. 3 we illustrate the results by using the analytical solution of (8). The results

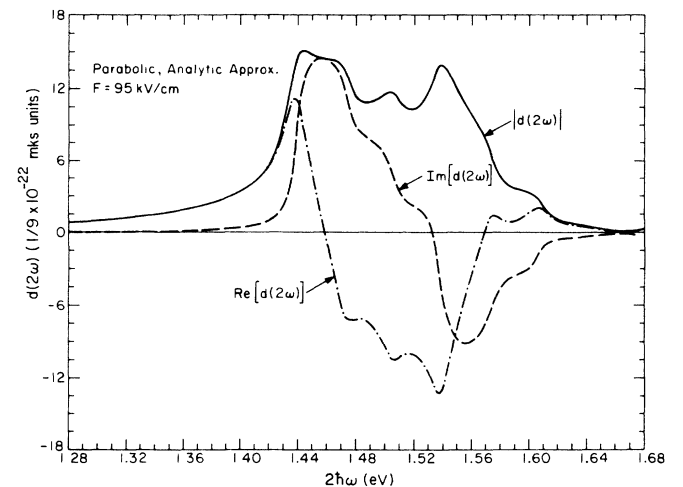


FIG. 3. The second-harmonic coefficient  $d(2\omega)$  as calculated by using the analytical formula of Eq. (8) of the parabolic-band model. The real part, imaginary part, and absolute value of  $d(2\omega)$  are plotted as functions of  $2\hbar\omega$  (eV). The parameters are  $L_w = 100 \text{ \AA}$  and  $L_w + L_B = 152 \text{ \AA}$ .

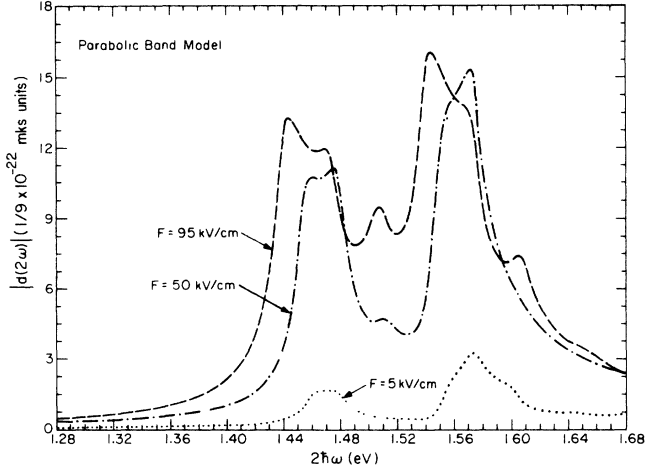


FIG. 4. The second-harmonic coefficient  $|d(2\omega)|$  ( $\frac{1}{9} \times 10^{-22}$  mks units) as a function of  $2\hbar\omega$  (eV) for  $L_w = 100$  Å and  $L_w + L_B = 152$  Å based on a parabolic-band model. The results of  $F = 5, 50,$  and  $95$  kV/cm are compared.

are generally in good agreement with those of Fig. 2. The differences between the two results occur because the analytical formula is based on a Taylor expansion with  $|E_n^c - E_l^c|$  and  $|E_l^{hh} - E_m^{hh}|$  as small parameters compared with  $\hbar\omega$ . This is not quite true. In our case,  $\hbar\omega$  is about  $0.7$  eV while  $E_n^c - E_l^c$  can be as large as  $0.25$  eV. This accounts for the difference between the two results.

In Fig. 4, we compare the results of  $|d(2\omega)|$  for different applied fields of  $5, 50,$  and  $95$  kV/cm based on the parabolic-band model. We note that the second-harmonic coefficient  $d(2\omega)$  decreases with the electric field. There is also a shift in resonant frequency due to the quantum-confinement Stark effect. The lower electric field also has fewer resonances because some of the transitions are forbidden at the vanishing electric field.

In Fig. 5, we illustrate the results based on the valence-band model of Eq. (24). The valence-subband

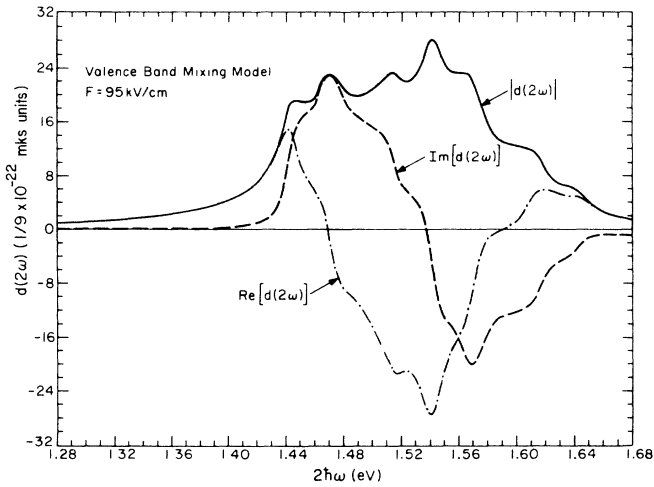


FIG. 5. The second-harmonic coefficient  $d(2\omega)$  ( $\frac{1}{9} \times 10^{-22}$  mks units) as a function of  $2\hbar\omega$  (eV) based on the valence-band-mixing model. The parameters are  $L_w = 100$  Å and  $L_w + L_B = 152$  Å and  $F = 95$  kV/cm.

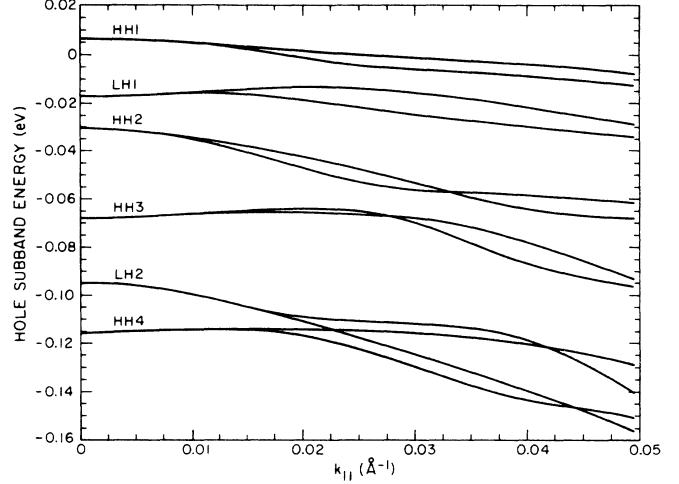


FIG. 6. Valence-band structure for a quantum well  $L_w = 100$  Å with an applied electric field  $F = 95$  kV/cm. The energies of the quantized states are plotted as a function of  $k_{||}$  (in Å $^{-1}$ ).

structure of the hole subband energies for the same parameters is shown in Fig. 6. For nonzero  $k_{||}$ , the increasing admixture of light- and heavy-hole states gives rise to strong nonparabolicities in the valence-band structure. Such coupling between heavy- and light-hole states also gives rise to a larger second-harmonic coefficient than the parabolic-band model. Comparing the results of Figs. 2 and 5 indicates that the result of the valence-band-mixing model is about a factor of 2 larger.

In Fig. 7, we compare the results of the valence-band-mixing model for different applied fields of  $F = 50, 95,$  and  $150$  kV/cm. We note that the second-harmonic coefficient generally increases with  $F$ . However, the peak value is saturated beyond a certain value of  $F$ . This occurs because for a large  $F$  the envelope functions of the conduction band and the valence band are pushed to different sides of the quantum well, reducing the value of

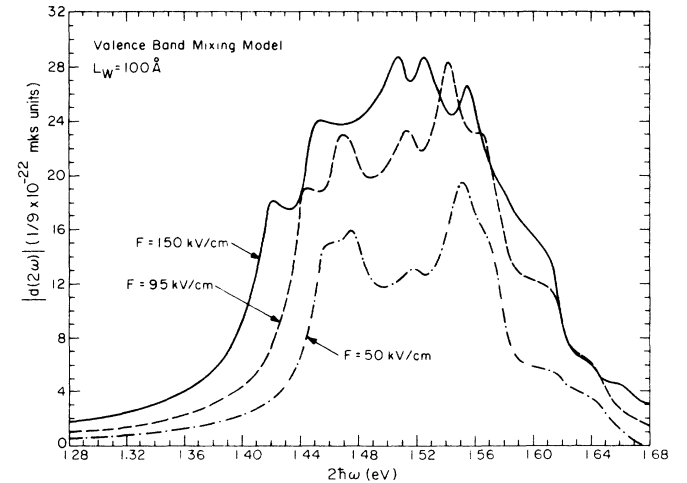


FIG. 7. The second-harmonic coefficient  $|d(2\omega)|$  ( $\frac{1}{9} \times 10^{-22}$  mks units) as a function of  $2\hbar\omega$  (eV) based on the valence-band-mixing model. The results of  $F = 50, 95,$  and  $150$  kV/cm are compared. The parameters of the quantum well are  $L_w = 100$  Å and  $L_w + L_B = 152$  Å.

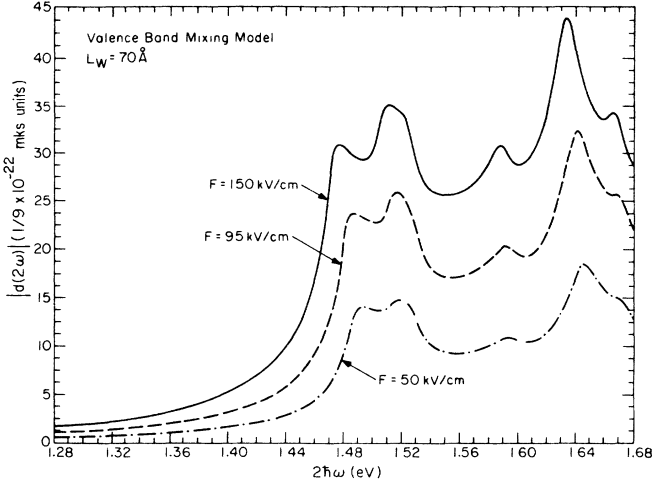


FIG. 8. The second-harmonic coefficient  $|d(2\omega)|$  ( $\frac{1}{9} \times 10^{-22}$  mks units) as a function of  $2\hbar\omega$  (eV) based on the valence-band-mixing model for a quantum well of  $L_w = 70$  Å and  $L_w + L_B = 106.4$  Å. The results of  $F = 50, 95,$  and  $150$  kV/cm are illustrated.

the overlap integral. We also see that the resonance shifts to a lower frequency for an increasing electric field.

In Fig. 8, we illustrate the results for a narrower quantum well of  $L_w = 70$  Å for  $F = 50, 95,$  and  $150$  kV/cm. The case of a narrower quantum well has a larger separation in intersubband energies and thus gives rise to a larger second-harmonic coefficient. [For example, in Eq. (24), if we set  $\epsilon_{\sigma_m m}^{cl}(k_{\parallel}) = \epsilon_{\sigma_m m}^{cn}(k_{\parallel})$ , then  $d(2\omega)$  is zero.] However, if the well becomes too narrow, then the higher-order subbands become unbounded. As can be seen from Eq. (24), we need at least a higher-order subband quantized state for  $d(2\omega)$  to be nonzero.

In Table I, we list the second-harmonic coefficient  $|d(2\omega)|$  as a function of electric field  $F$  for  $L_w = 100$  Å. To avoid resonant absorption, it is necessary to have a nonzero detuning  $\delta$  where  $2\hbar\omega = \epsilon_{U1}^{cl}(k_{\parallel} = 0) - \delta$ . We set the detuning at  $\delta = 0.075$  eV, which should be far enough from the resonant absorption. We have also listed the number of bound states  $n_c$  and  $n_v$  in the conduction band and valence band, respectively. We note that generally the second-harmonic coefficient increases with  $F$ .

The magnitudes of  $d(2\omega)$ , shown in Figs. 7 and 8 and Table I range from the order of 1 to 44 times ( $\frac{1}{9} \times 10^{-22}$  mks units). Note<sup>36</sup>  $1 \times (\frac{1}{9} \times 10^{-22} \text{ mks/units}) = 1.25 \times 10^{-12} \text{ m/V} = 3.0 \times 10^{-9} \text{ esu}$ . Thus the second-order coefficients for these GaAs/Al<sub>x</sub>Ga<sub>1-x</sub>As quantum-well structures are comparable to those of lithium niobate<sup>42</sup> ( $d_{31} \cong 4.76 \times \frac{1}{9} \times 10^{-22}$  mks units) and are substantially

TABLE I. Second-harmonic coefficient  $|d(2\omega)|$  as a function of electric field  $F$  for a quantum well with  $L_w = 100$  Å,  $L_w + L_B = 152$  Å. The frequency is such that  $2\hbar\omega = (\epsilon_{U1}^{cl}(k_{\parallel} = 0) - 0.075)$  eV.  $n_c$  denotes the number of bound states in a conduction band, and  $n_v$  denotes the number of bound states in a valence band of  $H^U$ .

Field (kV/cm)	$ d(2\omega) $ ( $\frac{1}{9} \times 10^{-22}$ mks units)	$n_c$	$n_v$
6	0.27	3	8
30	1.32	3	8
60	1.77	2	7
90	2.35	2	6
120	2.80	2	6
150	3.09	2	6

smaller than that of the bulk GaAs [ $d_{14} = d_{123} = (107 \pm 30) \times \frac{1}{9} \times 10^{-22}$  mks units]. Our numerical results agree in order of magnitude with those of Khurgin.<sup>16,28</sup> For experimental implementation of these nonlinear effects in quantum-well structures, the second-harmonic amplitude has a saturation value determined by the ratio of  $d(2\omega)$  and the absorption coefficient of the material at  $2\omega$  if the phase-matching condition is satisfied.<sup>43</sup> The length required to reach the saturation value is also determined by the inverse of the absorption coefficient. Thus it is important to optimize the second-harmonic-generation amplitude and the coupling (saturation) length by decreasing the absorption coefficient with a proper design of the quantum-well structure such that the absorption is small at the photon energy  $2\hbar\omega$  with a reasonable amount of detuning. More work is necessary for the experimental implementation of the nonlinear effects in quantum-well structures.

## V. CONCLUSIONS

In this paper, second-order nonlinear susceptibility in a quantum well with an applied electric field has been studied theoretically using both a parabolic-band model and a valence-band-mixing model. It is demonstrated that the nonlinear susceptibility can be enhanced significantly with an applied electric field across a symmetric quantum-well structure. The dispersion in both the real and the imaginary parts of the second-order susceptibility is shown numerically using both models. The realistic band structure using the valence-band-mixing model should be used when accurate numerical results are desired, although the parabolic-band model is easier to use numerically and some rough numerical results may be obtained.

## APPENDIX A: DERIVATION OF EQ. (8)

To derive an analytical expression that approximates  $d(2\omega)$  for the parabolic-band model, we first replace the product of the two cosines in (7) by its average value of  $\frac{1}{2}$  and ignore the  $\hbar\gamma$ 's. Next we Taylor expand the integrand by assuming the intersubband separation  $|E_n^c - E_j^c|$  to be small for the first term in square brackets and, for the second term, we expand by assuming  $|E_m^{hh} - E_l^{hh}|$  to be small. Then

$$\begin{aligned}
d_{\text{zxx}}(2\omega) = & -\frac{|e|^3 P^2 m_r}{6\pi \hbar^2 L_s} \int_0^\infty dE \left[ \sum_{n,m} \sum_{l(\neq n)} \frac{\langle \phi_m^{\text{hh}} | \phi_n^c \rangle \langle \phi_n^c | z | \phi_l^c \rangle \langle \phi_l^c | \phi_m^{\text{hh}} \rangle}{(E + E_{\text{hhm}}^{\text{cn}})^3 (2\hbar\omega - E - E_{\text{hhm}}^{\text{cn}}) (\hbar\omega - E - E_{\text{hhm}}^{\text{cn}})^2} \right. \\
& \times (E_l^c - E_n^c) (2E + 2E_{\text{hhm}}^{\text{cn}} - \hbar\omega) \\
& - \sum_{n,m} \sum_{l(\neq m)} \frac{\langle \phi_m^{\text{hh}} | \phi_n^c \rangle \langle \phi_l^{\text{hh}} | z | \phi_m^{\text{hh}} \rangle \langle \phi_n^c | \phi_l^{\text{hh}} \rangle}{(E + E_{\text{hhm}}^{\text{cn}})^3 (2\hbar\omega - E - E_{\text{hhm}}^{\text{cn}}) (\hbar\omega - E - E_{\text{hhm}}^{\text{cn}})^2} \\
& \left. \times (E_l^{\text{hh}} - E_m^{\text{hh}}) (2E + 2E_{\text{hhm}}^{\text{cn}} - \hbar\omega) \right], \tag{A1}
\end{aligned}$$

where  $E_{\text{hhm}}^{\text{cn}} = E_n^c + E_m^{\text{hh}} + E_g$ . The first term in (A1) is of the form  $\int_0^\infty dE \sum_{n,m} \sum_{l(\neq n)} v(n, l, m, E)$  and can be manipulated as follows. It is first written as  $\int_0^\infty dE \sum_{n,m} \sum_{l(>n)} v(n, l, m, E) + \int_0^\infty dE \sum_{n,m} \sum_{l(>n)} v(l, n, m, E)$ . In the second integral, the dummy integration variable  $E$  is replaced by  $E' + E_n^c - E_l^c$ . It turns out that  $v(l, n, m, E' + E_n^c - E_l^c) = -v(n, l, m, E')$ . Hence, the two integrals combined to give

$$\int_0^{E_l^c - E_n^c} dE \sum_{n,m} \sum_{l(>n)} v(n, l, m, E).$$

The second term in (A1) can be manipulated in the same manner. Thus,

$$\begin{aligned}
d_{\text{zxx}}(2\omega) = & -\frac{|e|^3 P^2 m_r}{6\pi \hbar^2 L_s} \left[ \sum_{n,m} \sum_{l(>n)} \int_0^{E_l^c - E_n^c} dE \frac{\langle \phi_m^{\text{hh}} | \phi_n^c \rangle \langle \phi_n^c | z | \phi_l^c \rangle \langle \phi_l^c | \phi_m^{\text{hh}} \rangle (E_l^c - E_n^c) (2E + 2E_{\text{hhm}}^{\text{cn}} - \hbar\omega)}{(E + E_{\text{hhm}}^{\text{cn}})^3 (2\hbar\omega - E - E_{\text{hhm}}^{\text{cn}}) (\hbar\omega - E - E_{\text{hhm}}^{\text{cn}})^2} \right. \\
& - \sum_{n,m} \sum_{l(>m)} \int_0^{E_l^{\text{hh}} - E_m^{\text{hh}}} dE \frac{\langle \phi_m^{\text{hh}} | \phi_n^c \rangle \langle \phi_l^{\text{hh}} | z | \phi_m^{\text{hh}} \rangle \langle \phi_n^c | \phi_l^{\text{hh}} \rangle}{(E + E_{\text{hhm}}^{\text{cn}})^3 (2\hbar\omega - E - E_{\text{hhm}}^{\text{cn}})} \\
& \left. \times \frac{(E_l^{\text{hh}} - E_m^{\text{hh}}) (2E + 2E_{\text{hhm}}^{\text{cn}} - \hbar\omega)}{(\hbar\omega - E - E_{\text{hhm}}^{\text{cn}})^2} \right]. \tag{A2}
\end{aligned}$$

Equation (A2) can be integrated readily. A linewidth is also introduced in the resonant term. Thus, we have  $d_{\text{zxx}}(2\omega)$  as given in Eq. (8) with the function  $I(x)$  defined as follows:

$$I(x) = \frac{3}{4(\hbar\omega)^2} \left[ \frac{1}{x^2} + \frac{3}{\hbar\omega x} - \frac{1}{2(\hbar\omega)^2} \ln \frac{x - 2\hbar\omega - i\hbar\gamma}{x} \right] + \frac{1}{\hbar\omega} \left[ \frac{1}{2x^2} + \frac{3}{2\hbar\omega x} - \frac{3}{(\hbar\omega)^2} \right] \frac{1}{x - \hbar\omega}. \tag{A3}$$

## APPENDIX B: BASIS TRANSFORMATION

The basis in Luttinger-Kohn's paper is

$$\begin{aligned}
|\frac{3}{2}, \frac{3}{2}\rangle &= -\frac{1}{\sqrt{2}} |(X + iY)\uparrow\rangle, \quad |\frac{3}{2}, -\frac{1}{2}\rangle = \frac{1}{\sqrt{6}} |(X - iY)\uparrow\rangle + (\frac{2}{3})^{1/2} |Z\downarrow\rangle, \\
|\frac{3}{2}, \frac{1}{2}\rangle &= -\frac{1}{\sqrt{6}} (X + iY)\downarrow\rangle + (\frac{2}{3})^{1/2} |Z\uparrow\rangle, \quad |\frac{3}{2}, -\frac{3}{2}\rangle = \frac{1}{\sqrt{2}} |(X - iY)\downarrow\rangle.
\end{aligned} \tag{B1}$$

The new basis is

$$|1\rangle = \alpha |\frac{3}{2}, \frac{3}{2}\rangle - \alpha^* |\frac{3}{2}, -\frac{3}{2}\rangle, \quad |2\rangle = \beta |\frac{3}{2}, -\frac{1}{2}\rangle - \beta^* |\frac{3}{2}, \frac{1}{2}\rangle, \quad |3\rangle = \beta |\frac{3}{2}, -\frac{1}{2}\rangle + \beta^* |\frac{3}{2}, \frac{1}{2}\rangle, \quad |4\rangle = \alpha |\frac{3}{2}, \frac{3}{2}\rangle + \alpha^* |\frac{3}{2}, -\frac{3}{2}\rangle, \tag{B2}$$

where  $\alpha = \exp[i(3\pi/4 - 3\phi/2)]/\sqrt{2}$ ,  $\beta = \exp[i(-\pi/4 + \phi/2)]/\sqrt{2}$ , and  $\phi$  is the angle defined by  $k_x = k_{\parallel} \cos\phi$  and  $k_y = k_{\parallel} \sin\phi$ .

## APPENDIX C: EVALUATION OF MATRIX ELEMENTS IN (19)

The matrix elements in (19) can be calculated by using (1), (14), (15), and the relations in Appendix A. They are as follows:

$$\langle \psi_l^{\text{c}\uparrow}(\mathbf{k}_{\parallel}) | x | \psi_m^{\text{U}}(\mathbf{k}_{\parallel}) \rangle = -\frac{P}{\epsilon_{cl}(\mathbf{k}_{\parallel}) - \epsilon_m^{\text{U}}(\mathbf{k}_{\parallel})} \left[ \frac{\alpha}{\sqrt{2}} \langle \phi_{cl} | g_m^{(1)} \rangle - \frac{\beta}{\sqrt{6}} \langle \phi_{cl} | g_m^{(2)} \rangle \right], \tag{C1}$$

where  $P$  is given in (4),

$$\langle \psi_l^{c\dagger}(\mathbf{k}_{\parallel}) | x | \psi_m^L(\mathbf{k}_{\parallel}) \rangle = \frac{P}{\varepsilon_{cl}(\mathbf{k}_{\parallel}) - \varepsilon_m^L(\mathbf{k}_{\parallel})} \left[ \frac{\beta}{\sqrt{6}} \langle \phi_{cl} | g_m^{(3)} \rangle - \frac{\alpha}{\sqrt{2}} \langle \phi_{cl} | g_m^{(4)} \rangle \right], \quad (C2)$$

$$\langle \psi_l^{c\dagger}(\mathbf{k}_{\parallel}) | x | \psi_m^U(\mathbf{k}_{\parallel}) \rangle = \frac{P}{\varepsilon_{cl}(\mathbf{k}_{\parallel}) - \varepsilon_m^U(\mathbf{k}_{\parallel})} \left[ -\frac{\alpha^*}{\sqrt{2}} \langle \phi_{cl} | g_m^{(1)} \rangle + \frac{\beta^*}{\sqrt{6}} \langle \phi_{cl} | g_m^{(2)} \rangle \right], \quad (C3)$$

$$\langle \psi_l^{c\dagger}(\mathbf{k}_{\parallel}) | x | \psi_m^L(\mathbf{k}_{\parallel}) \rangle = \frac{P}{\varepsilon_{cl}(\mathbf{k}_{\parallel}) - \varepsilon_m^L(\mathbf{k}_{\parallel})} \left[ -\frac{\beta^*}{\sqrt{6}} \langle \phi_{cl} | g_m^{(3)} \rangle + \frac{\alpha^*}{\sqrt{2}} \langle \phi_{cl} | g_m^{(4)} \rangle \right], \quad (C4)$$

$$\langle \psi_l^{\sigma_l\dagger} | z | \psi_m^{\sigma_m} \rangle = \begin{cases} \sum_{\nu=1,2} \langle g_l^{(\nu)}(\mathbf{k}_{\parallel}) | z | g_m^{(\nu)}(\mathbf{k}_{\parallel}) \rangle & \text{if } \sigma_l = \sigma_m = U \\ \sum_{\nu=3,4} \langle g_l^{(\nu)}(\mathbf{k}_{\parallel}) | z | g_m^{(\nu)}(\mathbf{k}_{\parallel}) \rangle & \text{if } \sigma_l = \sigma_m = L \\ 0 & \text{otherwise,} \end{cases} \quad (C5)$$

$$\langle \psi_n^{c\eta_n} | z | \psi_l^{c\eta_l} \rangle = \delta_{\eta_n \eta_l} \langle \phi_n^c | z | \phi_l^c \rangle. \quad (C6)$$

<sup>1</sup>L. Esaki and R. Tsu, IBM J. Res. Dev. **14**, 61 (1970).

<sup>2</sup>L. Esaki and L. L. Chang, Phys. Rev. Lett. **33**, 495 (1974).

<sup>3</sup>R. Dingle, W. Wiegmann, and C. H. Henry, Phys. Rev. Lett. **33**, 827 (1974).

<sup>4</sup>R. Tsu, L. L. Chang, G. A. Sai-Haiasz, and L. Esaki, Phys. Rev. Lett. **34**, 1509 (1979).

<sup>5</sup>T. C. Sollner, W. D. Goodhue, P. E. Tannenwald, C. D. Parker, and D. D. Peck, Appl. Phys. Lett. **43**, 588 (1983).

<sup>6</sup>D. A. B. Miller *et al.*, Phys. Rev. Lett. **53**, 2173 (1984).

<sup>7</sup>D. A. B. Miller *et al.*, Phys. Rev. B **32**, 1043 (1985).

<sup>8</sup>N. Holonyak, Jr. *et al.*, IEEE J. Quantum Electron. **QE-16**, 170 (1980).

<sup>9</sup>W. T. Tsang, Appl. Phys. Lett. **40**, 217 (1982).

<sup>10</sup>B. F. Levine *et al.* Appl. Phys. Lett. **50**, 1092 (1987).

<sup>11</sup>F. Capasso, in *Applications of Multiquantum Wells, Selective Doping, and Superlattices*, Vol. 24 of *Semiconductors and Semimetals*, edited by R. Dingle (Academic, New York, 1987), Chap. 6.

<sup>12</sup>S. L. Chuang and K. Hess, J. Appl. Phys. **59**, 2885 (1986); **61**, 1510 (1987).

<sup>13</sup>D. A. B. Miller, D. S. Chemla, T. C. Damen, A. C. Gossard, W. Wiegmann, T. H. Wood, and C. A. Burrus, Appl. Phys. Lett. **45**, 13 (1984).

<sup>14</sup>J. S. Wiener *et al.* Appl. Phys. Lett. **49**, 531 (1986).

<sup>15</sup>Y. C. Chang, J. Appl. Phys. **58**, 499 (1985).

<sup>16</sup>J. Khurgin, Appl. Phys. Lett. **51**, 2100 (1987); Phys. Rev. B **38**, 4056 (1988).

<sup>17</sup>D. Ahn and S. L. Chuang, J. Appl. Phys. **62**, 3052 (1987).

<sup>18</sup>D. Ahn and S. L. Chuang, IEEE J. Quantum Electron. **QE-23**, 2196 (1987).

<sup>19</sup>F. H. Julien *et al.* Appl. Phys. Lett. **53**, 116 (1988).

<sup>20</sup>D. A. B. Miller *et al.* Appl. Phys. Lett. **41**, 679 (1982).

<sup>21</sup>D. S. Chemla, D. A. B. Miller, and P. W. Smith, Ref. 11, Chap. 5.

<sup>22</sup>M. Yamanishi, Phys. Rev. Lett. **59**, 1014 (1987).

<sup>23</sup>D. S. Chemla, D. A. B. Miller, and S. Schmitt-Rink, Phys. Rev. Lett. **59**, 1018 (1987).

<sup>24</sup>D. A. B. Miller, J. E. Henry, A. C. Gossard, and J. H. English, Appl. Phys. Lett. **49**, 821 (1986).

<sup>25</sup>D. A. B. Miller, Appl. Phys. Lett. **54**, 202 (1989).

<sup>26</sup>M. K. Gurnick and T. A. DeTemple, IEEE J. Quantum Electron. **QE-19**, 791 (1983).

<sup>27</sup>L. Tsang, D. Ahn, and S. L. Chuang, Appl. Phys. Lett. **52**, 697 (1988).

<sup>28</sup>J. Khurgin, J. Appl. Phys. **64**, 5026 (1988).

<sup>29</sup>D. E. Aspnes, Phys. Rev. B **6**, 4648 (1972).

<sup>30</sup>C. Y. Fong and Y. R. Shen, Phys. Rev. B **12**, 2325 (1975).

<sup>31</sup>D. J. Moss, J. E. Sipe, and H. M. van Driel, Phys. Rev. B **36**, 1153 (1987).

<sup>32</sup>D. J. Moss, J. E. Sipe, and H. M. van Driel, Phys. Rev. B **36**, 9708 (1987).

<sup>33</sup>D. Ahn, S. L. Chuang, and Y. C. Chang, J. Appl. Phys. **64**, 4056 (1988).

<sup>34</sup>D. Ahn and S. L. Chuang, J. Appl. Phys. **64**, 6143 (1988).

<sup>35</sup>N. Bloembergen, *Nonlinear Optics* (Benjamin, New York, 1965).

<sup>36</sup>Y. R. Shen, *The Principles of Nonlinear Optics* (Wiley, New York, 1984).

<sup>37</sup>E. O. Kane, J. Phys. Chem. Solids **1**, 249 (1957).

<sup>38</sup>M. Asada, A. Kameyama, and Y. Suematus, IEEE J. Quantum Electron. **QE-20**, 745 (1984).

<sup>39</sup>Y. Kan, H. Nagai, M. Yamanishi, and I. Suemune, IEEE J. Quantum Electron. **QE-23**, 2167 (1987).

<sup>40</sup>J. M. Luttinger and W. Kohn, Phys. Rev. **97**, 869 (1955).

<sup>41</sup>D. A. Broido and L. J. Sham, Phys. Rev. B **31**, 888 (1985).

<sup>42</sup>A. Yariv, *Optical Electronics*, 3rd ed. (Holt, Rinehart, and Winston, New York, 1985), p. 233.

<sup>43</sup>J. Khurgin, J. Opt. Soc. Am. Ser. B **6**, 1673 (1989).